Phys Chem Minerals (2006) 33: 217–226
DOI 10.1007/s00269-006-0070-5

ORIGINAL PAPER

Hitoshi Yusa · Masaki Akaogi · Nagayoshi Sata
Hiroshi Kojitani · Ryo Yamamoto · Yasuo Ohishi

High-pressure transformations of ilmenite to perovskite, and lithium niobate to perovskite in zinc germanate

Received: 31 October 2005 / Accepted: 2 February 2006 / Published online: 8 March 2006

Abstract In-situ X-ray powder diffraction measurements conducted under high pressure confirmed the existence of an unquenchable orthorhombic perovskite in $ZnGeO_3$. $ZnGeO_3$ ilmenite transformed into perovskite at 30.0 GPa and 1300 ± 150 K in a laser-heated diamond anvil cell. After releasing the pressure, the lithium niobate phase was recovered as a quenched product. The perovskite was also obtained by recompression of the lithium niobate phase at room temperature under a lower pressure than the equilibrium phase boundary of the ilmenite–perovskite transition. Bulk moduli of ilmenite, lithium niobate, and perovskite phases were calculated on the basis of the refined X-ray diffraction data. The structural relations among these phases are considered in terms of the rotation of GeO_6 octahedra. A slight rotation of the octahedra plays an important role for the transition from lithium niobate to perovskite at ambient temperature. On the other hand, high temperature is needed to rearrange GeO_6 octahedra in the ilmenite–perovskite transition. The correlation of quenchability with rotation angle of GeO_6 octahedra for other germanate perovskites is also discussed.

H. Yusa (✉)
Advanced Materials Laboratory, National Institute for Materials Science, 1-1 Namiki, Tsukuba, 305-0044, Ibaraki, Japan
E-mail: yusa.hitoshi@nims.go.jp
Tel.: +81-298-8604420
Fax: +81-298-8527449

M. Akaogi · H. Kojitani · R. Yamamoto
Department of Chemistry, Gakushuin University, 1-5-1 Mejiro, Toshima-ku, 171-8588, Tokyo, Japan

N. Sata
Institute for Research on Earth Evolution,
Japan Agency for Marine-Earth Science and Technology, 2–15, Natsushima-cho, Yokosuka, 237–0061, Kanagawa, Japan

Y. Ohishi
Japan Synchrotron Radiation Research Institute, 1–1-1 Kouto, Mikazuki-cho, Sayo-gun, 679–5198, Hyogo, Japan

Keywords Perovskite · Lithium niobate · Ilmenite · X-ray diffraction · High-pressure phase transition

Introduction

Some high-pressure perovskites in ABO_3 compounds exhibit unquenchable phenomena during decompression to atmospheric pressure. There are two types of instability: one is amorphization [e.g. $CaSiO_3$ (Mao et al. 1989), $SrSiO_3$ (Yusa et al. 2005)], and the other is conversion into the lithium niobate phase from the perovskite phase [e.g. $MgGeO_3$ (Leinenweber et al. 1994), $MnTiO_3$ (Ross et al. 1989)]. It is believed that such instability is closely correlated with the ionic radii of A^{2+} and B^{4+} cations forming the perovskite structure. The Goldschmidt tolerance factor (e.g. Mitchell 2002), $t = (r_A + r_o)/\sqrt{2}\,(r_B + r_o)$, where r denotes the effective ionic radii (Shannon 1976) of each element, not only substantially indicates the distortion from an ideal cubic perovskite; it is also applicable to such instabilities during decompression. In the former case, the tolerance factor is close to or greater than unity ($CaSiO_3$: $t = 0.990$; $SrSiO_3$: $t = 1.045$), where the large A^{2+} cation might destroy the perovskite structure and change it into the amorphous state during decompression. On the other hand, Leinenweber et al. (1994) suggests that for $t < 0.84$ (e.g. $MgGeO_3$: $t = 0.839$; $MnTiO_3$: $t = 0.832$), the perovskite phase converts to the lithium niobate phase. If the perovskite structure is stable in the $ZnGeO_3$ composition, the value ($t = 0.843$) should be close to the limit of the unquenchable perovskite in germanate, considering that $MnGeO_3$ perovskite ($t = 0.865$) are quenchable (Liu 1976). From the perspective of comparative crystallography, the existence of $ZnGeO_3$ perovskite is significant in regard to the quenchability of the perovskite group.

The low-pressure phase in $ZnGeO_3$ is ilmenite, which has been confirmed in a sample recovered from high P-T synthesis (Ringwood and Major 1967; Syono et al. 1971). Even at ambient pressure, no pyroxene phase

exists, but the mixture of Zn_2GeO_4 (phenacite structure) and GeO_2 (rutile structure) is stable. The post-ilmenite phase was surveyed by Liu (1977) and by Ito and Matsui (1979). Liu (1977) proposed an orthorhombic phase for the product recovered from a laser-heated sample in a diamond anvil cell at 24 GPa and 1,000–1,400°C. On the other hand, Ito and Matsui (1979) showed that $ZnGeO_3$ ilmenite transforms into a corundum structure at 20–30 GPa, judging from the quenched products. They also reported on high-pressure synthesis of corundum-type $MgGeO_3$, which was later confirmed by Leinenweber et al. (1994) to be the lithium niobate phase recovered from an unquenchable perovskite. From the crystallographic viewpoint, the lithium niobate structure ($R3c$) is an ordered derivative of the corundum structure ($R\bar{3}c$) in which both A^{2+} and B^{4+} cations are found in the same layer perpendicular to c axis. Therefore, the corundum phase indicated by Ito and Matsui (1979) would have actually been the lithium niobate phase. Recently, Akaogi et al. (2005) determined the phase boundary between the ilmenite and post-ilmenite phases, which was recovered as the lithium niobate phase, to be P(GPa) = 27.4–0.0032 T(K). Until now, however, no one has reported perovskite as a post-ilmenite phase in the $ZnGeO_3$ composition. We used in-situ X-ray diffraction to confirm the existence of a perovskite structure in a $ZnGeO_3$ composition under pressure and at high temperature. As has been indicated for $MgGeO_3$, $MnTiO_3$, and $FeTiO_3$ (Leinenweber et al. 1991, 1994; Ross et al. 1989), the recompression experiments show that the lithium niobate phase has a reversible transition to perovskite at room temperature with a small kinetic barrier. We think a similar transition may occur in the $ZnGeO_3$ composition. Hence, a recompression experiment on the lithium niobate phase was also carried out.

Experimental methods

The starting sample of $ZnGeO_3$ ilmenite was prepared from an equimolar mixture of ZnO and GeO_2 by using a Kawai-type multianvil apparatus applying a pressure and temperature of 10 GPa and 1,200°C for 2 h (Akaogi et al. 2005). The lattice parameters determined from the powder X-ray diffraction pattern indicated that $a = 4.960$ Å, and $c = 13.864$ Å, which are in good agreement with the values reported by Syono et al. (1971) and Ross and Leinenweber (1990). The product had a brownish color due to a color center probably derived from point defects. The high-pressure experiment was conducted in a diamond anvil cell (DAC). The sample was put into a hole (0.15 mm in diameter.) in a rhenium gasket (0.07 mm in thickness) without any pressure medium. A few small grains of ruby were enclosed in the sample for the pressure measurement. The sample in the gasket was placed on the diamond anvil and compressed to the target pressure at room temperature. The in-situ X-ray diffraction experiments under high pressure were carried out at SPring-8 (Japan Synchrotron Radiation Research Institute). The Nd:YLF laser heating system installed on the beam line (BL10XU) was used in the high P–T experiments. The temperature was monitored from the spectroscopic measurements of radiation emitted from the sample during heating. The angle dispersive X-ray diffraction was detected by using an imaging plate (IP), which provides precise d-values as well as intensity data. The wavelength of the incident X-ray beam was tuned to 0.41284 Å by using an Si(111) monochrometer and was collimated to 20 μm in diameter at the sample position ($L = 446.86$ mm). A wide conical aperture of the tungsten carbide seating the diamond anvil made it possible to collect Debye rings up to 17.5° in 2θ. Further experimental details are described elsewhere (Watanuki et al. 2001; Yusa et al. 2005).

The recompression experiments on the recovered sample were performed at room temperature on another beam line (BL04B2) at SPring-8. The laser-heated sample was taken off the gasket and broken into fine fragments by using a needle. A fragment together with a ruby pressure marker was dropped into a hole (0.2 mm in diameter.) in another gasket (0.09 mm in thickness). The sample was immersed in a pressure medium (methanol:ethanol:water = 13:3:1) to present a quasi-hysrostatic condition. The distance from the IP to the sample was kept as long as possible ($L = 593.04$) in the X-ray diffractometer so that a high-energy X-ray ($\lambda = 0.32900$ Å) could be used to get an accurate value for d. A 50-micron collimator was used, and the average exposure time was 20 min. All X-ray diffraction images were converted with a computer program (fit-2D; Hammersley 1997) into one-dimensional X-ray profiles plotted as a function of 2θ.

Results

Ilmenite–perovskite transition under high pressure and temperature

When the pressure reached 30 GPa, we focused Nd:YLF laser at the center of the sample on both sides for 10 min. The temperature of the heated spot (30 μm in diameter) was 1,300 ± 150 K. The heated area became transparent. The pressure dropped to 26 GPa after heating. The X-ray diffraction peaks were sharp rather than the broad peaks of the ilmenite phase of the unheated area (Figs. 1b and 2b). We continued to heat the sample to obtain a single phase of the transparent product after applying more pressure (34 GPa) to compensate for the pressure relaxation caused by the phase transition. In this heating, the entire sample area was repeatedly scanned by the laser beam for 50 min and the temperature was kept within 1,500 K. The X-ray diffraction profiles indicated that the sample had completely changed into the new phase and that the peaks became sharp (Figs. 1b, c and 2b, c). Although there were many overlapping peaks, an individual profile fit-

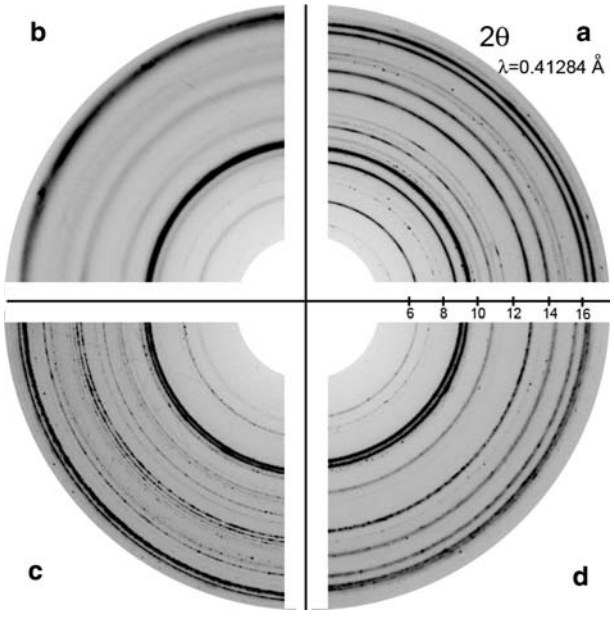

Fig. 1 X-ray diffraction images collected by IP. A part of the Debye rings are shown in quarter sectors for four different conditions: **a** Before compression. **b** At 30 GPa before laser heating. **c** At 31.5 GPa after the final stage of laser heating. **d** After decompression to ambient pressure. All images were taken from the sample in a diamond anvil cell at room temperature

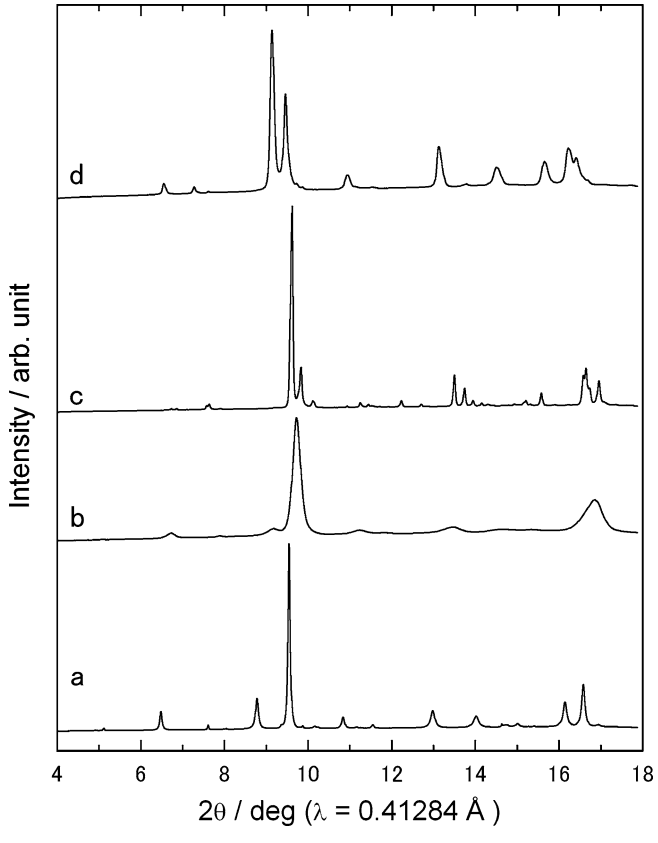

Fig. 2 Integrated diffraction profiles of the IP: **a** Before compression. **b** At 30 GPa before laser heating. **c** At 31.5 GPa after the final stage of laser heating. **d** After decompression to ambient pressure

ting based on Pseudo-Voigt peak function indicated that the powder pattern can be assigned as index of an orthorhombic perovskite structure (*Pbnm*), which is denoted as d_{obs} in Table 1. However, it is very difficult to resolve individual overlapping peaks such as (020) and (112). The whole powder pattern decomposition (the Le Bail method by GSAS: Larson and Von Dreele 2004) was used to refine the lattice parameters. As indicated in Fig. 3, the fitting analysis converged with $R_w = 0.035$. The refined lattice parameters were determined to be $a = 4.8190$ Å, $b = 4.9479$ Å, $c = 7.0278$ Å and $V = 167.57$ Å^3 at 31.5 GPa. For this refinement, we did not use the results of the Rietvelt analysis because the spotty Debye ring and non-hydrostatic condition influenced the diffraction peaks' intensity and thus including them would have resulted in a large error ($R_w = 0.101$). The stability of the perovskite phase was checked during the decompression to ambient pressure (at 20.7, 10.7, and 5.2 GPa) at room temperature. No sign of transition was evident during the decompression to 20.7 GPa. However at 10.7 GPa, the perovskite phase began to change into another phase and had completely changed by the time

Table 1 X-ray powder diffraction data for $ZnGeO_3$ perovskite

H	*k*	*l*	d_{obs} (Å)	d_{cal} (Å)
1	0	1		3.9744
0	0	2	3.5122	3.5139
1	1	0	3.4514	3.4522
1	1	1	3.0956	3.0986
0	2	0		2.4740
1	1	2	2.4633	2.4626
2	0	0	2.4114	2.4095
0	2	1	2.3398	2.3336
1	2	0		2.2009
2	1	0	2.1688	2.1663
1	2	1		2.1003
1	0	3	2.1032	2.1069
2	1	1	2.0660	2.0702
0	2	2		2.0229
2	0	2		1.9872
1	1	3	1.9367	1.9384
1	2	2	1.8637	1.8652
2	1	2	1.8440	
0	0	4	1.7552	1.7570
2	2	0	1.7247	1.7261
0	2	3	1.6995	1.7010
2	2	1	1.6747	1.6763
1	2	3		1.6040
2	1	3		1.5905
1	3	0	1.5600	1.5604
3	0	1		1.5659
1	1	4		1.5658
2	2	2	1.5476	1.5493
3	1	0		1.5278
1	3	1	1.5217	1.5233
3	1	1		1.4930
1	3	2	1.4245	1.4261
0	2	4	1.4303	1.4325
2	0	4	1.4184	1.4196
3	1	2	1.3998	1.4011

Orthorhombic, probable space group *Pbnm* ($Z = 4$) $a = 4.8190$ Å, $b = 4.9479$ Å, $c = 7.0278$ Å, $V = 167.57$ Å^3 ($R_w = 0.035$) at 31.5 GPa

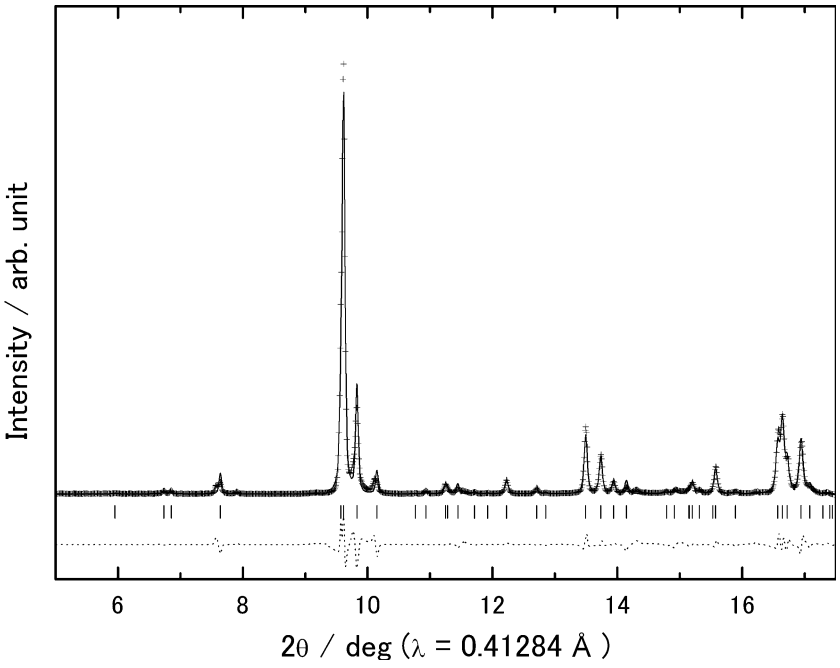

Fig. 3 Powder X-ray diffraction pattern fitting by the Le Bail method. The observed pattern (*crosses*) has the same profile as Fig. 2c. The difference (*dotted line*) between the observed and fitted pattern (*thin line*) is also shown on the same scale. Background was subtracted. *Vertical bars* represent the calculated positions of the diffraction peaks of the orthorhombic perovskite phase

5.2 GPa had been reached. Moreover, it existed at atmospheric pressure (Figs. 1d and 2d). The diffraction peaks of the phase were indexed by using the lithium niobate structure ($R3c$), not the ilmenite structure ($R\bar{3}$). This is the same type of phase change as happens to $MgGeO_3$ perovskite (Leinenweber et al. 1994). A visible change in the sample occurred during decompression. The transmittance of light gradually decreased around 12 GPa. This phenomenon was similar to the one observed in the $MgGeO_3$ perovskite transition. According to transmission electron microscopy observations of $MgGeO_3$ perovskite (Leinenweber et al. 1994), it can be attributed to the formation of twin boundaries undergoing a phase transition to the lithium niobate structure. The details of this transition under quasi-hydrostatic pressure are described below.

Recompression experiment on lithium niobate phase at room temperature

In the recompression experiments, the X-ray diffraction patterns were taken after making stepwise increases in pressure. Figure 4 shows several diffraction profiles taken under different pressures. Rietvelt analysis (GSAS: Larson and Von Dreele 2004) was used to refine the structure and lattice parameters. Since a small amount of ilmenite (less than 5%) from the unheated portion near the gasket remained in the recovered sample, the multiple phase analysis of GSAS was able to simultaneously analyze the ilmenite phase together with lithium niobate and/or perovskite phases. Figure 5 shows observed and fitted X-ray diffraction patterns as an illustration of the GSAS analysis. For the isotropic thermal parameters (U_{iso}) of perovskite, fixed values of the $ZnGeO_3$ ilmenite, which were derived from a single-crystal structure refinement (Ross and Leinenweber 1990), were used to avoid the inappropriate convergence of U_{iso} in the calculation. The lattice parameters of the recovered phase at ambient pressure were determined to be $a = 5.013$ Å, and $c = 13.021$ Å, indicating a lithium niobate structure ($R3c$) with $R_w = 0.0185$. These values were also in good accord with the "corundum" phase (Ito and Matsui 1979) described above, which has $a = 5.0128$ Å, and $c = 13.0219$ Å.

During the compression at room temperature without heating, the phase gradually changed to orthorhombic perovskite (*Pbnm*). The structure is the same as that formed from laser heating of ilmenite under high pressure. When the pressure reached 19.2 GPa, the lithium niobate phase completely disappeared from the diffraction profile. Table 2 lists the atomic coordinates of the perovskite structure as determined by the Rietvelt analysis. Figure 6 shows a crystallographic drawing of perovskite based on the present atomic coordination.

The symptom of the change into perovskite phase appears at 13.3 GPa (Fig. 4a). This pressure was considerably lower than the phase boundary of the ilmenite–perovskite transition, which passes across 26.5 GPa at room temperature (Akaogi et al. 2005). The perovskite phase gradually reverted to the lithium niobate phase with decreasing pressure. Note that the perovskite clearly remained at 10.6 GPa in the decompression process, while the perovskite could not be seen at the same pressure in the compression process (Fig. 4a). In addition, the lithium niobate phase survived at 15.6 GPa during compression whereas it did not appear in the diffraction pattern taken at 14.7 GPa during decompression (Fig 4b). Phase fractions of perovskite and lithium niobate can be obtained by Rietvelt analysis. These fractions in the compression and decompression process are separately shown in Fig. 7. These facts

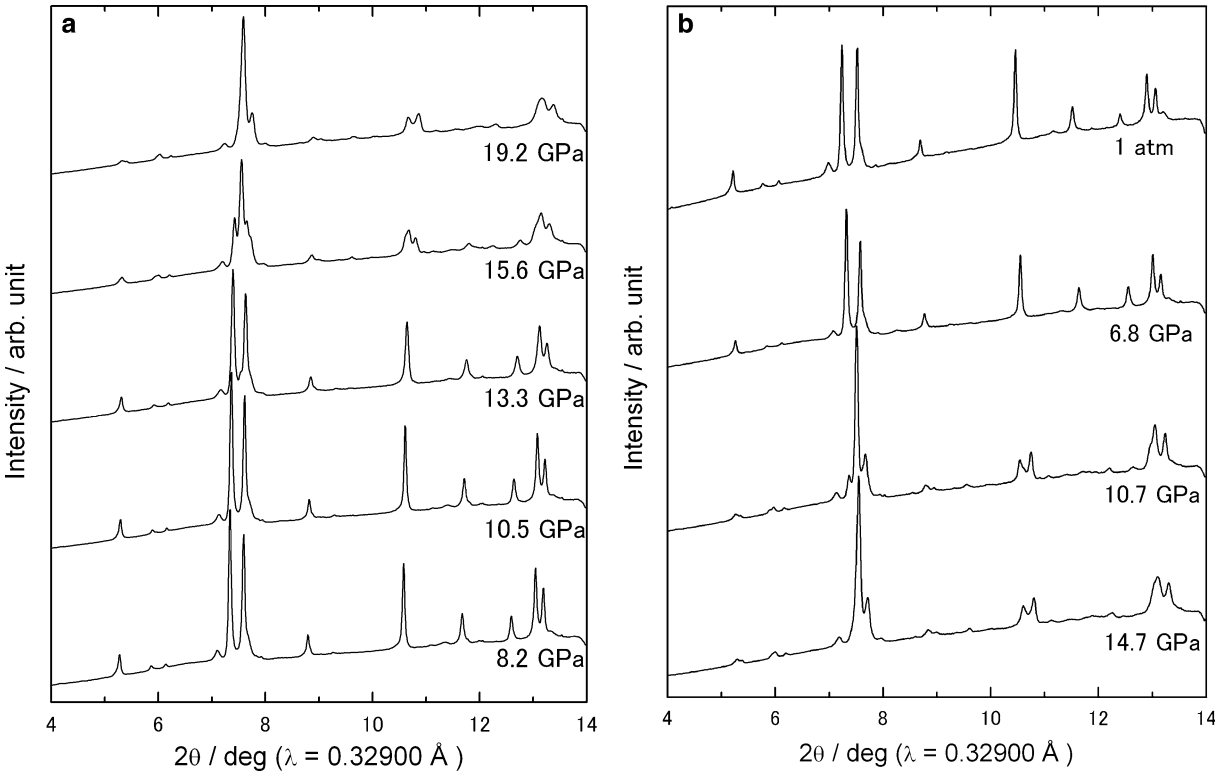

Fig. 4 X-ray diffraction patterns of the recompression experiment on the lithium niobate phase. **a** Compression process. **b** Decompression process

indicate the same type of kinetic hysteresis as reported for $MgGeO_3$ and $MnTiO_3$ (Leinenweber et al. 1994; Ross et al. 1989). The volume difference between perovskite and lithium niobate can be directly compared at the same pressure because of the sluggish transformation at room temperature. Table 3 summarizes the volumes of lithium niobate and perovskite for different pressures. At 15.6 GPa, the volume change from lithium niobate to perovskite is 2.3%. This is comparable to the reported difference of 3% for $MgGeO_3$ (Leinenweber et al. 1994). The analysis was able to obtain the volume difference between ilmenite and perovskite because un-

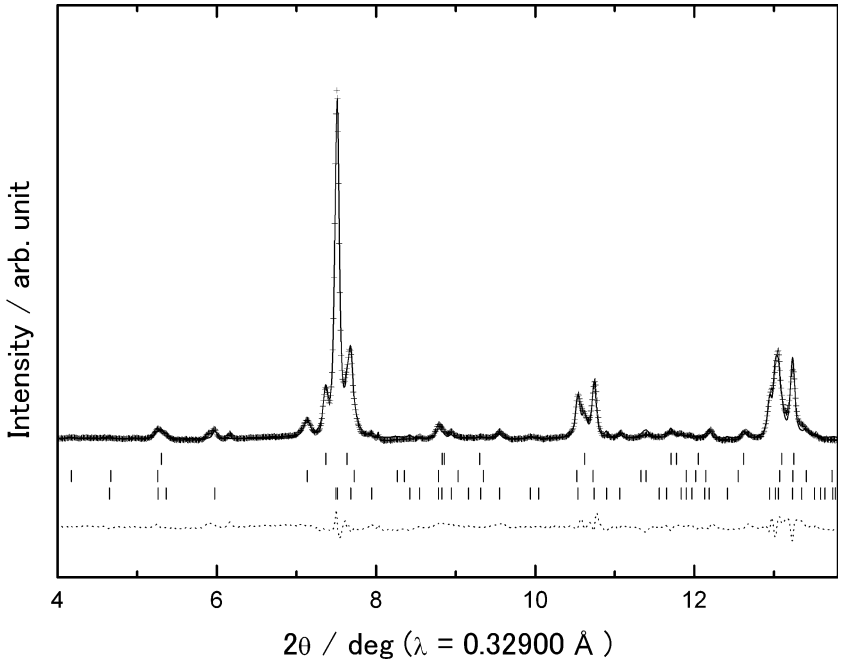

Fig. 5 Multiple phase analysis by using the Rietveld method (GSAS) for the mixture phase of ilmenite, lithium niobate, and perovskite at 10.7 GPa at room temperature. The difference (*dotted line*) between the observed and fitted pattern (*thin line*) is also shown on the same scale. Background was subtracted. *Vertical bars* represent the calculated positions of the diffraction peaks; top, lithium niobate; intermediate, ilmenite; bottom orthorhombic perovskite. $R_w = 0.023$

Table 2 Refined atomic coordinates for $ZnGeO_3$ perovskite at 19.2 GPa

Atom	*X*	*y*	*z*
Zn	0.5133	0.5385	0.25
Ge	0.5	0	0.5
O1	0.1327	0.4230	0.25
O2	0.1802	0.1881	0.5612

transformed ilmenite was mixed with the sample. The difference, 5.5%, is more than twice as large as the difference between lithium niobate and perovskite. Figure 8 plots the volume data per formula unit. The zero-pressure volume of the perovskite can be calculated from extrapolation. The difference between ilmenite and perovskite expands to 6.6% at ambient pressure. The volume changes from 6 to 8% are commonly associated with the ilmenite–perovskite transition in the other ABO_3 compounds, such as $MgSiO_3$, $MnGeO_3$ (e.g. Ito and Matsui 1979). On the other hand, the quenchable orthorhombic phase reported by Liu (1977) exhibits very small volume change (0.2%) from ilmenite phase. Although he implied the quenched phase can be indexed by *Pbmn* perovskite, such a small volume change is generally inappropriate for the ilmenite–perovskite transition. Moreover, the observed intensity by Liu (1977) is clearly inconsistent with the calculated intensity of $ZnGeO_3$ perovskite. For example, in the Liu's table, 40 are given as the relative intensity (I/I_{100}) of (110) reflection with *d*-spacing of 3.61 Å; however, according to the calculation, the intensity should be less than 1. Instead, (012) reflection of lithium niobate could fit into the *d*-spacing of 3.61 Å with acceptable intensity. On the above reason, we think that the identification of the quenchable perovskite by Liu (1977) might be full of question marks.

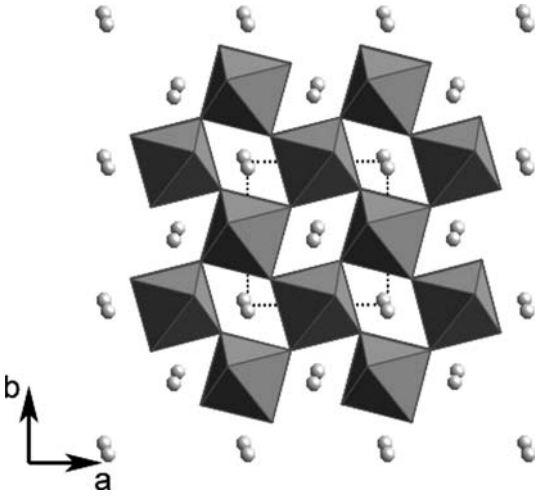

Fig. 6 Projection of the orthorhombic perovskite structure in $ZnGeO_3$ along the *c* axis at 19.2 GPa. The unit cell is indicated by the *dotted line*

Discussion

Bulk moduli of ilmenite, lithium niobate and perovskite

The bulk moduli of ilmenite, lithium niobate, and perovskite were calculated by fitting the volume data to the Birch–Murnaghan equation of state. To make up for the dispersed data, we assumed K′ to be 4 in all calculations. Table 4 summarizes the calculated bulk moduli. The compression curves of ilmenite and lithium niobate phase were interpolated with all volume data under

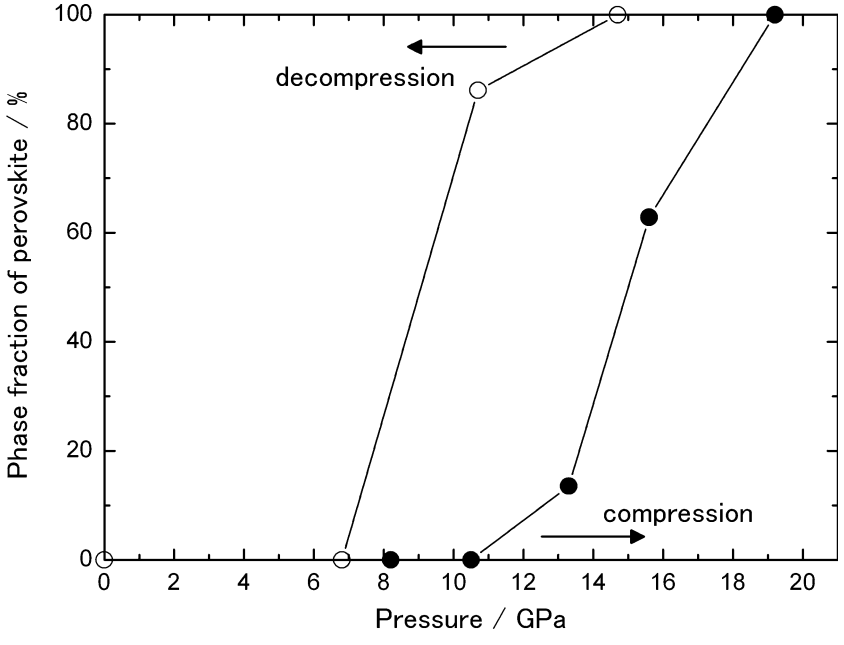

Fig. 7 Phase fractions of perovskite with increasing and decreasing pressure at ambient temperature. *Solid and open symbols* indicate the phase fractions in the compression and decompression process, respectively

Table 3 Lattice parameters and volumes of lithium niobate and perovskite under quasi-hydrostatic pressure

P (GPa)	Phase	*a* (Å)	*b* (Å)	*c* (Å)	*V* (Å^3)
2.9	Lithium niobate	4.9941		12.9381	279.46
5.6	Lithium niobate	4.9777		12.8669	276.09
8.2	Lithium niobate	4.9647		12.8133	273.52
10.5	Lithium niobate	4.9533		12.7615	271.16
13.3	Lithium niobate	4.9410		12.7011	268.53
	Perovskite	4.8963	5.0251	7.1114	174.97
15.6	Lithium niobate	4.9265		12.6418	265.71
	Perovskite	4.8796	5.0129	7.1233	174.24
19.2	Perovskite	4.8657	4.9968	7.0829	172.21
14.7	Perovskite	4.8890	5.0152	7.1293	174.81
10.7	Perovskite	4.9116	5.0324	7.1657	177.11
	Lithium niobate	4.9394		12.7829	270.09
6.8	Lithium niobate	4.9767		12.8492	275.60
0.0	Lithium niobate	5.0137		13.0211	283.46
	Perovskite[a]				184.13[a]

[a]Extrapolated from high pressure data, see text

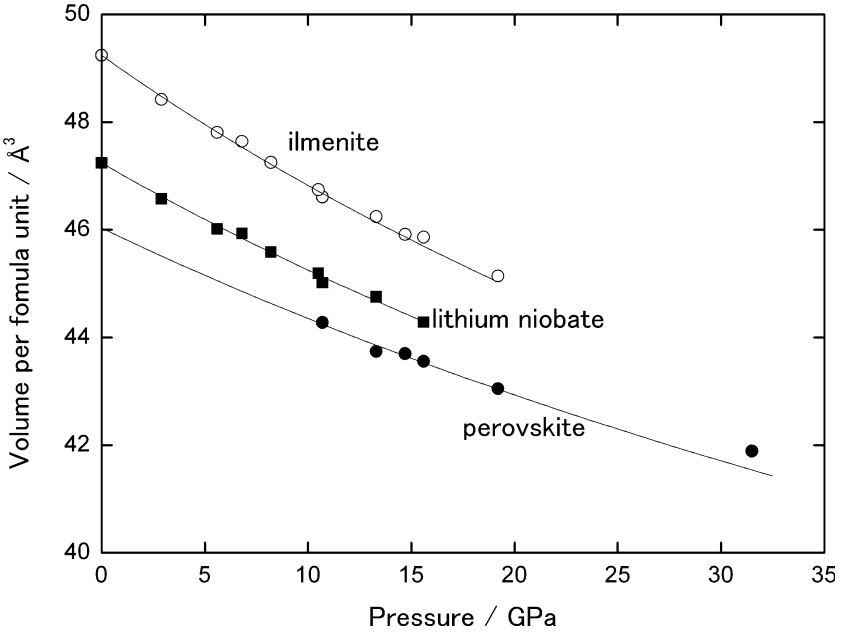

Fig. 8 Pressure–volume data of $ZnGeO_3$ ilmenite, lithium niobate, and perovskite. *Open circles*, *solid squares*, and *solid circles* represent ilmenite, lithium niobate, and perovskite phases, respectively. All volume data are normalized per formula unit. The compression curve (*solid line*) was obtained by fitting the data to the Birch–Murnaghan equation of state

Table 4 Bulk moduli, K_0(GPa) of germante, titanate and stannate ilmenite, lithium niobate and perovskite

Compound	Ilmenite	Lithium niobate	Perovskite
$ZnGeO_3$	180(2)[a]	213(3)[a]	250(3)[a]
$MgGeO_3$	187(2)[b]	213(10)[c]	–
$MnTiO_3$	170(9)[d]	158(9)[d]	227(4)[d]
$MnSnO_3$	–	205(7)[e]	257(18)[e]
$FeTiO_3$	177(3)[f]	182(7)[g] 218(4)[e]	236[e]

[a]This study
[b]Sato et al. (1977)
[c]Leinenweber et al. (1994)
[d]Ross et al. (1989)
[e]Leinenweber et al. (1991)
[f]Wechsler and Prewitt (1984)
[g]Mehta et al. (1994)

quasi-hydrostatic pressure. Because of the unquenchable behavior, the curve for perovskite was determined by extrapolating to zero pressure. The zero-pressure volume in Table 3 was obtained from this calculation. We removed the volume at the highest pressure from the calculation because the non-hydrostatic condition without any pressure medium causes uncertainty. If the volume is included in the calculation, a rather high value, $K_0 = 289(4)$ GPa, is obtained. The compounds listed in Table 4 also have the isostructural phase of ilmenite, lithium niobate, and perovskite. Considering the systematics of bulk moduli in these compounds, the present compound of $ZnGeO_3$ has reasonable bulk moduli values.

Structural relations among ilmenite, lithium niobate and perovskite

The crystal structures of ilmenite and lithium niobate are similar in that both are ordered derivatives of the corundum structure. Therefore, crystal model drawings

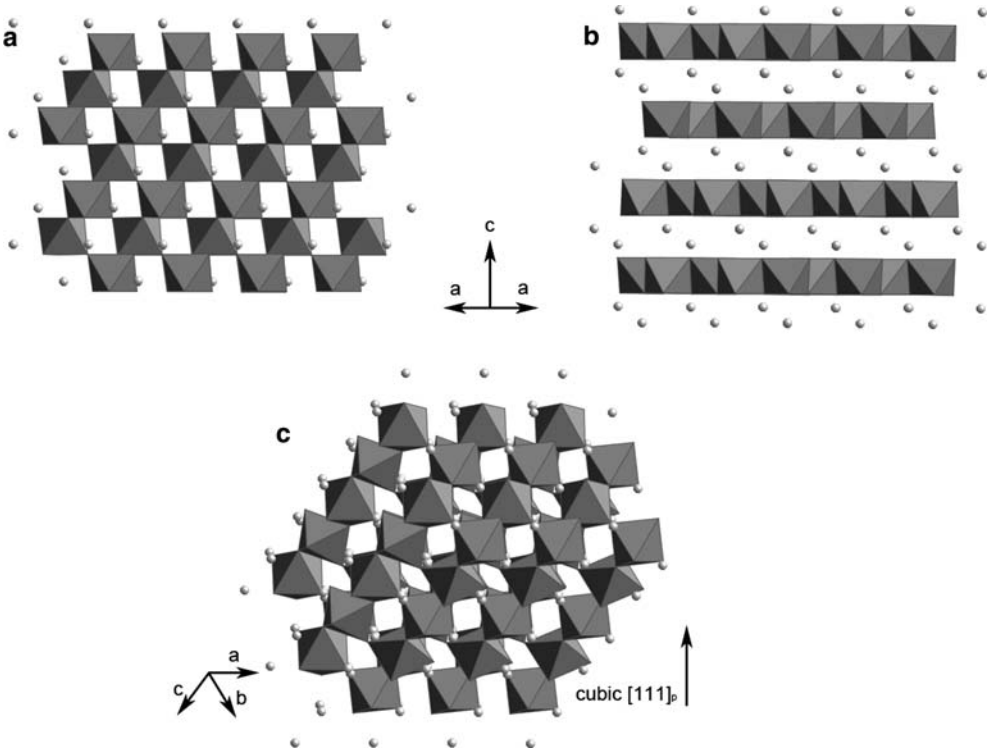

Fig. 9 Structural relations among ilmenite, lithium niobate, and perovskite. Projections perpendicular to the *c* axis of lithium niobate (**a**) and ilmenite (**b**) are shown. A triad axis $[111]_p$ of a pseudocubic perovskite lattice is indicated in the orthorhombic perovskite structure (**c**)

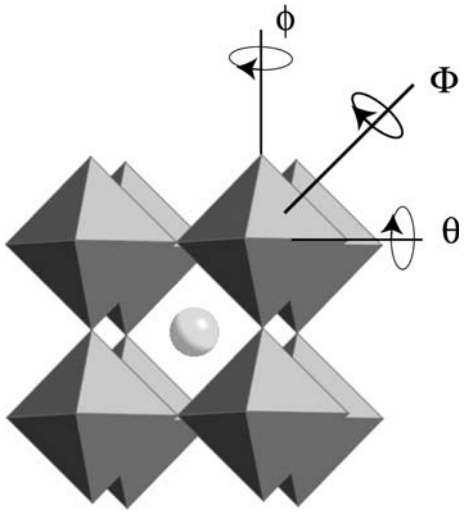

Fig. 10 Directions of the rotation and tilting axes. The orthorhombic distortion to the *Pbnm* perovskite is defined by two octahedral tiltings of θ about $[110]_p$ and φ about $[001]_p$. The rotation Φ represents the [111] direction of the BO_6 octahedra in the pseudocubic perovskite cell

from a specific crystallographic orientation (Fig. 9) are useful to understand the transformations of ilmenite or lithium niobate into perovskite. The models are drawn with the same orientation, taking into account GeO_6 octahedra. As can be seen in the figure, the transformation from lithium niobate to perovskite is much easier than that from ilmenite to perovskite. In other words, a large displacement has to be given to GeO_6 octahedra in order to trigger the ilmenite–perovskite transition, where the atomic rearrangements should be controlled by diffusion under high temperature. No change from the ilmenite phase was observed throughout the pressure range at room temperature. As suggested by Ross et al. (1989) for the $MnTiO_3$ composition, unlike the ilmenite–perovskite transition, the lithium niobate–perovskite transition is induced without a large-scale diffusion of 8–12 coordinated cations. The structural change requires only a small rotation of the TiO_6 octahedron. The same transition scheme would be plausible for the lithium niobate–perovskite transition in $ZnGeO_3$.

Megaw (1968) notes that it is possible to transform an octahedral framework continuously from the ideal cubic perovskite configuration to the lithium niobate configuration as the tilt angle increases. O'Keeffe et al. (1979) suggests that a single rotation Φ about the triad axis $[111]_p$ of a pseudocubic perovskite lattice can be represented as a rotation of the BO_6 octahedra as indicated in Fig. 10. The angle can be calculated from the atomic coordinates (Zhao et al. 1993b; Mitchell 2002) or estimated from the cell dimensions (O'Keeffe et al. 1979; Zhao et al. 1993a). In the present $ZnGeO_3$ composition, the calculated rotation angle is 21.8° for lithium niobate at 13.3 GPa and 19.4° for perovskite at 15.6 GPa. Note that the difference is only 2.4°. This small difference might lead to lithium niobate changing into perovskite under metastable conditions at room temperature.

Systematics of other germanate perovskites

Several orthorhombic perovskites were found in other $A^{2+}GeO_3$ compounds, such as $CaGeO_3$, $CdGeO_3$,

Table 5 Lattice parameters and tilting angle of BO_6 octahedra in orthorhombic perovskite structure

Compound	a (Å)	b (Å)	c (Å)	Φ (deg)	A^{2+} radii (Å)	References
$CaGeO_3$	5.2607	5.2688	7.4452	3.9	1.12	Sasaki et al. (1983)
$CdGeO_3$	5.209	5.253	7.434	10.7	1.10	Susaki (1989)
$MnGeO_3$	5.084	5.214	7.323	16.8	0.96	Liu (1976)
$ZnGeO_3$ (15.6 GPa)	4.8796	5.0129	7.1233	19.4	0.90	This study
$MgGeO_3$ (17.9 GPa)	4.832	5.031	7.022	20.8	0.89	Leinenweber et al. (1994)
$CaTiO_3$	5.3796	5.4423	7.6401	10.2	1.12	Sasaki et al. (1987)
$CdTiO_3$	5.3053	5.4215	7.6176	15.5	1.10	Sasaki et al. (1987)
$MnTiO_3$ (4.45 GPa)	5.1048	5.3046	7.4180	20.5	0.96	Ross et al. (1989)
$FeTiO_3$ (16.2 GPa)	5.04	5.17	7.27	17.1	0.92	Leinenweber et al. (1991)
(Mg, Fe) TiO_3 (21 GPa)	4.9852	5.2104	7.2305	21.1	0.905[a]	Linton et al. (1999)
$CdSnO_3$	5.547	5.577	7.867	7.3	1.10	Smith (1960)
$MnSnO_3$ (7.35 Gpa)	5.301	5.445	7.690	18.4	0.96	Leinenweber et al. (1991)

[a]Average radii of Mg^{2+} and Fe^{2+}

$MnGeO_3$, and $MgGeO_3$ (Sasaki et al. 1983; Susaki 1989; Liu 1976; Leinenweber et al. 1994). The rotation angle (Φ) also indicates the degree of distortion from an ideal cubic perovskite ($\Phi = 0$). We have investigated the systematic relationship between the effective ionic radii of A^{2+} and Φ for germanate perovskites. The lattice parameters and Φ are summarized in Table 5. The perovskites in $ZnGeO_3$ and $MgGeO_3$ are unquenchable. The table lists their high-pressure values. In germanate perovskites, the smaller radii of the A^{2+} cation needs a larger rotation of the GeO_6 octahedron for an orthorhombic perovskite structure to be stabilized. In the case of $CaGeO_3$ perovskite, which contains the relatively large Ca^{2+} cation, only 3.9° is required for the rotation. As shown in Fig. 11, the plots of A^{2+} radii versus Φ indicate a definite correlation. The boundary to change into lithium niobate would be located around 17°–18°, because $MnGeO_3$ perovskite is known to be quenchable (Liu 1976).

Leinenweber et al. (1994) concluded that unquenchable perovskites, which convert into lithium niobate, have a tolerance factor less than 0.84, based on the systematics of the tolerance factor in germanate. From the effective ionic radii of eight-coordinated Zn^{2+} and of six-coordinated Ge^{4+}, it appears that $ZnGeO_3$ would have a limiting value of $t = 0.843$. Their discussion assumed the effective ionic radii for the ambient condition. However, the pressure effect on the ionic radii should be included in this kind of discussion, although it is difficult to obtain the pressure dependence of ionic radii. In contrast, the discussion on quenchability based on the rotation Φ has advantages that the value can be obtained under pressure and the rotation directly reflects the distortion from the perovskite structure. In the case of $ZnGeO_3$, the rotation is not sensitive to pressure, which varies only from 18.9° to 19.4° in the pressure range. As is clearly seen in Fig. 11, the unquenchability of ABO_3 perovskite to lithium niobate is correlated to the rota-

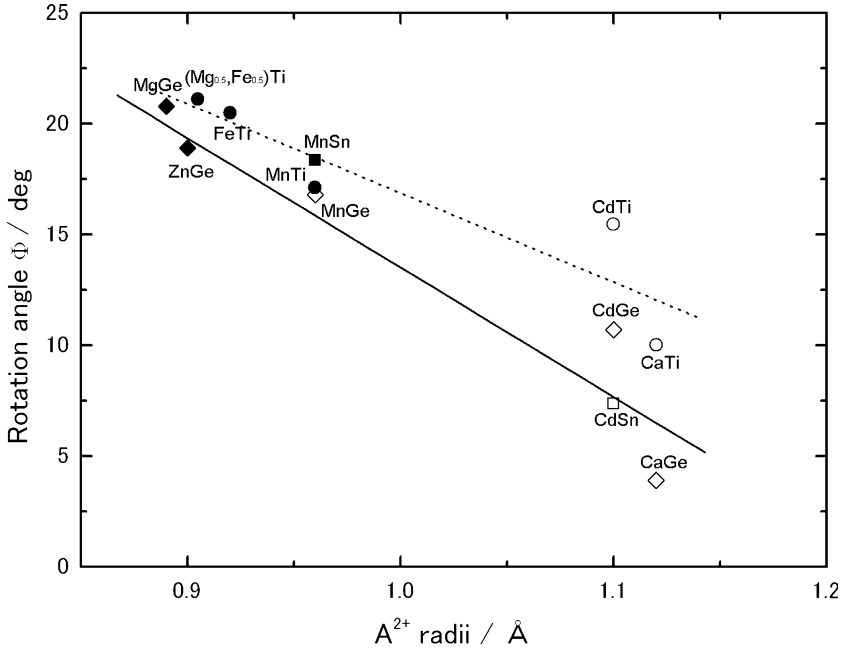

Fig. 11 Relation between effective ionic radii of eight-coordinated A^{2+} and the rotation angle in germanate (*diamond symbol*), titanate (*circle symbol*), and stannate (*square symbol*) perovskites. Symbols with AB indicate ABO_3 perovskites. *Solid* and *dotted lines* show the linear fittings of germanates and titanates group, respectively. *Solid symbols* indicate that the perovskites converts into the lithium niobate structure on releasing pressure

tion of $B^{4+}O_6$ octahedra and the ionic radii of A^{2+}. The lithium noiabate phase is concentrated in the region of higher rotation angle and smaller ionic radii. Both germanates and titanates have the same tendency, but the germanates' ionic radii exhibit a rather strong dependency on the rotation angle. This result shows that if the octahedra rotation extends beyond a certain limit, it will stabilize the lithium niobate structure as the pressure is reduced.

Acknowledgements The synchrotron radiation experiments were performed at SPring-8 with the approval of the Japan Synchrotron Radiation Research Institute (JASRI). We are grateful to N. Funamori and an anonymous reviewer for constructive comments on the manuscript.

References

Akaogi M, Kojitani H, Yusa H, Yamamoto R, Kido M, Koyama K (2005) High-pressure transitions and thermochemistry of $MGeO_3$ (M = Mg, Zn, and Sr) and Sr-silicates: systematics in enthalpies of formation of $A^{2+}B^{4+}O_3$ perovskites. Phys Chem Miner 32:603–613

Hammersley AP (1997) Fit-2d: in introduction and overview. European Synchrotron Radiation Facility Internal Report ESRF97HA02T

Ito E, Matsui Y (1979) High-pressure transformation in silicates. germanates, and titanates with ABO_3 stoichiometry. Phys Chem Miner 4:265–273

Larson AC, Von Dreele RB (2004) General structure analysis system (GSAS), Los Alamos National Laboratory Report LAUR 86:748

Leinenweber K, Utsumi W, Tsuchida Y, Yagi T, Kurita K (1991) Unquenchable high-pressure perovskite polymorph of $MnSnO_3$ and $FeTiO_3$. Phys Chem Miner 18:244–250

Leinenweber K, Wang Y, Yagi T, Yusa H (1994) An unquenchable perovskite phase of $MgGeO_3$ and comparison with $MgSiO_3$ perovskite. Am Miner 79:197–199

Linton JA, Fei Y, Navrotsky A (1999) The $MgTiO_3$-$FeTiO_3$ join at high pressure and temperature. Am Miner 84:1595–1603

Liu L (1976) High-pressure phase of Co_2GeO_4, Ni_2GeO_4, Mn_2GeO_4 and $MnGeO_3$: implication for the germanate-silicate modeling scheme and the earth's mantle. Earth Planet Sci Lett 31:393–396

Liu L (1977) Post-ilmenite phases of silicates and germanates. Earth Planet Sci Lett 35:161–168

Mao H-K, Chen LC, Hemley RJ, Jephcoat AP, Wu Y (1989) Stability and equation of state of $CaSiO_3$-perovskite to 134 Gpa. J Geophys Res 94:17889–17894

Megaw HD (1968) A note on the structure of lithium niobate, $LiNbO_3$. Acta Cryst 24:583–588

Mehta A, Leinenweber K, Navrotsky A, Akaogi M (1994) Calorimetric study of high pressure polymorphism in $FeTiO_3$: stability of the perovskite phase. Phys Chem Miner 21:207–212

Mitchell RH (2002) Perovskites: modern and ancient. Almaz Press Inc., Ontario

O'Keeffe M, Hyde BG, Bovin J-O (1979) Contribution to the crystal chemistry of orthorhombic perovskites: $MgSiO_3$ and $NaMgF_3$. Phys Chem Miner 4:299–305

Ringwood AE, Major A (1967) High pressure transformation in zinc germanates and silicates. Nature 215:1367–1368

Ross NL, Leinenweber K (1990) Single crystal structure refinement of high-pressure $ZnGeO_3$ ilmenite. Z Kristallo 191:93–104

Ross NL, Ko J, Prewitt CT (1989) A new phase transtion in $MnTiO_3$: $LiNbO_3$-perovskite structure. Phys Chem Miner 16:621–629

Sasaki S, Prewitt CT, Liebermann (1983) The crystal structure of $CaGeO_3$ perovskite and the crystal chemistry of the $GdFeO_3$-type perovskites. Am Miner 68:1189–1198

Sasaki S, Prewitt CT, Bass JD (1987) Orthorhombic perovskite $CaTiO_3$ and $CdTiO_3$: structure and space group. Acta Cryst 43:1668–1674

Sato Y, Ito E, Akimoto S (1977) Hydrostatic compression of ilmenite phase of $ZnSiO_3$ and $MgGeO_3$. Phys Chem Miner 2:171–176

Shannon RD(1976) Revised effective ionic radii and systematic studies of interatomic distances in halides and chalcogenides. Acta Cryst 32: 751–767

Smith AJ(1960) The system cadmium oxide-stannic oxide. Acta Cryst 13:749–752

Susaki J (1989) $CdGeO_3$-phase transformations at high pressure and temperature and structural refinement of the perovskite polymorph. Phys Chem Miner 16:634–641

Syono Y, Akimoto S, Matsui Y (1971) High pressure transformation in zinc silicates. J Solid State Chem 3:369–380

Watanuki T, Shimomura O, Yagi T, Kondo T, Isshiki M (2001) Construction of laser-heated diamond anvil cell system for in-situ x-ray diffraction study at SPring-8. Rev Sci Instrum 72:1289–1292

Wechsler BA, Prewitt CT (1984) Crystal structure of ilmenite ($FeTiO_3$) at high temperature and at high pressure. Am Miner 69:176–185

Yusa H, Akaogi M, Sata N, Kojitani H, Kato Y, Ohishi Y (2005) Unquenchable hexagonal perovskite in high-pressure polymorphs of storontium silicates. Am Miner 90:1017–1020

Zhao Y, Weidner DJ, Parise JB, Cox DE (1993a) Thermal expansion and structural distortion of perovskite—data for $NaMgF_3$ perovskite. Part I. Phys Earth Planet Inter 76:1–16

Zhao Y, Weidner DJ, Parise JB, Cox DE (1993b) Critical phenomena and phase transition of perovskite—data for $NaMgF_3$ perovskite. Part II. Phys Earth Planet Inter 76:17–34